Thermodynamic and structural properties of the thin radiating surface layer of a white dwarf

Riccardo Fantoni[*]
Università di Trieste, Dipartimento di Fisica, strada Costiera 11, 34151 Grignano (Trieste), Italy
(Dated: September 11, 2026)

We determine thermodynamic and structural properties of the Coulomb plasma (jellium) in the thin surface layer of a white dwarf using the path integral Monte Carlo method within a general relativity description of the star.

Keywords: White dwarf;Jellium;Path Integral;Monte Carlo;General Relativity;Thin surface layer;Thermodynamics;Structure

CONTENTS

I. INTRODUCTION

White dwarfs [1] are the dense remnants of stars, composed mainly of carbon and oxygen nuclei, which contain electrons, protons and neutrons and are supported against collapse induced by gravity by the electron degeneracy pressure due to Pauli exclusion principle. They remain white dwarfs till gravity overcomes electron degeneracy pressure, crushing electrons into protons to form neutrons through β^+ decay.

Therefore the simplest model for the interior of a white dwarf is that of *Jellium*. This is a system of pointwise electrons immersed in a uniform neutralizing background. The density of the electron gas is so high that the Fermi temperature is much higher than the temperature of the star and the electron gas can be considered degenerate. Chandrasekar [2–5] model of a white dwarf equilibrium structure didn't take into account the effects of general relativity. First Tolman [6], and later Oppenheimer and Volkoff [7] proposed a way to treat the hydrodynamic equations for the equilibrium and stability of a star within the framework of general relativity.

The luminosity of a white dwarf is due to a thin radiating layer on the star surface (see chapter 4 of the book [1]). The mechanism of a white dwarf cooling is the primary bridge between our theoretical description of the star and observational data which rely on essentially two aspects: luminosity observations and time scale of the observed cooling.

---

[*] riccardo.fantoni@scuola.istruzione.it

Purpose of this work is to determine the properties of the electron plasma in this thin surface layer using the path integral Monte Carlo (PIMC) method [8] at low non zero temperature. In order to take into account the effects of general relativity we will use the $3+1$ foliation of Arnowitt, Deser, and Misner (ADM) [9] to build a density matrix from the stress-energy tensor through a path integral where on each imaginary timeslice one selects a constant time foil [10]. This amounts to treat the quantum Coulomb plasma in the classical Schwarzschild spatial metric in a patch of subatomic dimensions at the radius $\mathscr{R}$ of the star of mass $\mathscr{M}$. In weak gravity the determinant ${}^3g$ of the spatial components of the metric tensor is such that $-\ln\sqrt{{}^3g} \approx -\ln(r^2|\cos\theta|) - \Phi/c^2$ with $\Phi = GM/r$ the Newtonian *gravitational potential*. We propose to use a *geometrical potential* acting on each electron $w = -\hbar[\ln\sqrt{g}]/\tau$ with τ the imaginary time step used in the discretization of the path integral. On the other hand we will neglect the physical gravitational potential of the gravitating electrons that should otherwise be included through the introduction of the Tolman-Ehrenfest temperature [11, 12].

The problem of the plasma on the surface of a sphere, has already been treated in Refs. [13–15]. Here the two dimensional curved surface of the sphere is substituted by the three dimensional spatial Schwarzschild foil of the white dwarf.

We may assume that the electrons dispersion relation is the one of non relativistic particles $\epsilon(p) = p^2/2m$. This is reasonable since the density of the electron-proton plasma [1] in the thin surface layer is $\rho_l \approx 10^3\mathrm{g/cm}^3$ (see section 4.1 of the book [1]) much lower than the central densities. Therefore $p_F^2/m^2c^2 \approx 0.01$ where m is the electron mass and $p_F = h(3n/4\pi)^{1/3}$ is the polarized electrons Fermi momentum. The temperature of the surface layer falls in the range $10^6\mathrm{K} \lesssim T \lesssim 10^7\mathrm{K}$. We will consider a white dwarf with a radius $\mathscr{R} \approx 700\mathrm{Km}$ and a mass $\mathscr{M} \approx 2\times 10^{30}\mathrm{Kg}$, so the Schwarzschild radius is about $R_{\mathrm{Sc}} \approx 3\mathrm{Km}$.

We will determine the effect of temperature, quantum statistics, gravity, and of imposing charge neutrality on the weakly correlated electron plasma in the quantum regime. The plasma we are confronting with move from the lower left corner of the phase diagram of figure 1 of Ref. [16] for the Euclidean jellium.

In the rest of this work we will use natural Planck units $c = G = \hbar = k_B = 1$ where c is the speed of light, $\hbar$ is the reduced Planck constant, G is the gravitational constant, and k_B is the Boltzmann constant.

II. ADM FOLIATION AND SCHWARZSCHILD METRIC

By Birkhoff theorem the vacuum solution of Einstein field equations outside a mass $\mathscr{M}$ is the one of Schwarzschild. Within the ADM foliation [9, 17] in imaginary time

$$||g_{\alpha\beta}|| = \begin{pmatrix} N^2 + N^iN_i & N_i \\ N_i & g_{ij} \end{pmatrix}, \tag{2.1}$$

the *shift* $N_i = 0$, the *lapse* $N^2 = (1 - R_{\mathrm{Sc}}/r)$, and $g_{rr} = (1 - R_{\mathrm{Sc}}/r)^{-1}, g_{\theta\theta} = r^2, g_{\varphi\varphi} = r^2\cos^2\theta$ with $R_{\mathrm{Sc}} = 2\mathscr{M}$ the Schwarzschild radius. We will generally use a Greek index to denote one of the 4 spacetime components and a Roman index to denote one of the 3 spatial components. We will also introduce ${}^3g = \det\{g_{ij}\} = (1 - R_{\mathrm{Sc}}/r)^{-1}r^4\cos^2\theta > 0$ with $r \gg R_{\mathrm{Sc}}$. Where for a typical white dwarf $\mathscr{R}/R_{\mathrm{Sc}} \sim 10^3$.

III. PIMC IN A FOIL OF SCHWARZSCHILD METRIC

A many body system composed of N *distinguishable* particles of mass m with positions in $R = (\boldsymbol{r}_1, \boldsymbol{r}_2, \ldots, \boldsymbol{r}_N) = (\{\boldsymbol{r}_l\})$ where each position vector $\boldsymbol{r}_i = (r_l^1, r_l^2, r_l^3) = (\{r_l^j\}) = (\{r^{j_l}\})$ in 3 dimensions. On a foil of Schwarzschild solution (2.1) with spatial metric tensor $g_{ij}(\boldsymbol{r})$, the geodesic distance between two infinitesimally close points R and R' is $d\tilde{s}^2(R, R') = \sum_{l=1}^N ds^2(\boldsymbol{r}_l, \boldsymbol{r}_l')$ where $ds^2(\boldsymbol{r}, \boldsymbol{r}') = g_{ij}(\boldsymbol{r})(\boldsymbol{r} - \boldsymbol{r}')^i(\boldsymbol{r} - \boldsymbol{r}')^j$. Moreover,

$$\tilde{g}_{ij}(R) = g_{i_1j_1}(\boldsymbol{r}_1) \otimes \ldots \otimes g_{i_Nj_N}(\boldsymbol{r}_N), \tag{3.1}$$

$$\tilde{g}(R) = \prod_{l=1}^N {}^3g(\boldsymbol{r}_l), \tag{3.2}$$

[1] Assuming that the white dwarf is made up of a completely ionized plasma then we may write $\rho = \mu_e m_u n$ with n the electrons number density, m_u the atomic mass unit, and $\mu_e = A/Z$ with Z the atomic number and A the mass number, so that for example for a ^{4}He or a ^{12}C white dwarf $\mu_e = 2$ and for a ^{56}Fe white dwarf $\mu_e = 56/26 \approx 2.134$.

where $||\tilde{g}_{ij}||$ is a matrix made of N diagonal blocks $||g_{i_l j_l}||$ with $l = 1, 2, \ldots, N$. The Laplace-Beltrami operator on the manifold of dimension $3N$ is

$$\Delta_R = \tilde{g}^{-1/2}\nabla_i(\tilde{g}^{1/2}\tilde{g}^{ij}\nabla_j), \tag{3.3}$$

where $\nabla = \nabla_R$, $\tilde{g}^{ij}$ is the inverse of $\tilde{g}_{ij}$, i.e. $\tilde{g}_{ij}\tilde{g}^{jk} = \delta_i{}^k$ the Kronecker delta.

The Hamiltonian $\mathscr{H}$ of the N non relativistic particles will be

$$\mathscr{H} = -\lambda\Delta_R + V(R), \tag{3.4}$$

where $\lambda = 1/2m$ and $V(R)$ is the *Coulomb potential* energy of the system, that we here assume only a function of the particles positions and bounded from below.

The density matrix ρ of the system obeys to Bloch equation

$$\frac{\partial\rho(t)}{\partial t} = -\mathscr{H}\rho(t), \tag{3.5}$$

$$\rho(0) = \mathbb{1}, \tag{3.6}$$

where t is the imaginary time with dimension of the reciprocal of energy and $\mathbb{1}$ the identity matrix. Here the fully general relativistic case requires the use of the Tolman-Ehrenfest imaginary time [11, 12] $t_{\rm TE} = t\sqrt{\tilde{g}_{00}}$ which is required to take correctly into account the *gravitational potential energy* of the electrons in the non relativistic, weak gravity, classical limit. Here and in the following we will drop this distinction thereby neglecting the gravitational potential. The position representation of the density matrix is then obtained from $\rho(R, R'; t) = \langle R|\rho(t)|R'\rangle$ with $\langle R|R'\rangle = \delta(R - R')/\sqrt{\tilde{g}(R)}$ where δ is a $3N$ dimensional Dirac delta function. In the small imaginary time τ limit the position representation of the density matrix is [15]

$$\rho(R, R'; \tau) \propto \tilde{g}(R)^{-1/4}\sqrt{\mathscr{D}(R, R'; \tau)}\,\tilde{g}(R')^{-1/4}e^{\lambda\tau\mathscr{R}(R)/6}e^{-\mathscr{S}(R,R';\tau)}, \tag{3.7}$$

where $\mathscr{R} = 0$ is the scalar curvature of the Schwarzschild spatial foil [2], $\mathscr{S}$ the action, and $\mathscr{D}$ the van Vleck's determinant [19, 20]

$$\mathscr{D}_{\mu\nu} = -\nabla_\mu\nabla'_\nu\mathscr{S}(R, R'; \tau), \tag{3.8}$$

$$\det||\mathscr{D}_{\mu\nu}|| = \mathscr{D}(R, R'; \tau), \tag{3.9}$$

where $\nabla = \nabla_R$ and $\nabla' = \nabla_{R'}$. This determinant is the Jacobian of the transformation from the initial conditions given by fixing the pair of momentum and coordinate of each particle to the boundary conditions given by specifying the pair of initial and final coordinates needed in the coordinate representation. The square root of the van Vleck determinant factor takes into account the density of paths among the minimum extremal region for the action (see Chapter 12 of Ref. [20]). The two factors $\tilde{g}^{-1/4}$ are needed in order to have for the density matrix a bidensity for which the boundary condition to Bloch equation is simply a Dirac delta function. In the small $\tau \to 0$ limit [3] $\tilde{g}(R)^{-1/4}\sqrt{D(R, R'; \tau)}\,\tilde{g}(R')^{-1/4} \to (1/2\lambda\tau)^N$.

For the *action* $\mathscr{S}$, the *kinetic-action* $\mathscr{K}$, and the *inter-action* $\mathscr{U}$ we have [4]

$$\mathscr{S}(R, R'; \tau) = \mathscr{K}(R, R'; \tau) + \mathscr{U}(R, R'; \tau), \tag{3.10}$$

$$\mathscr{K}(R, R'; \tau) = \frac{dN}{2}\ln(4\pi\lambda\tau) + \frac{d\tilde{s}^2(R, R')}{4\lambda\tau}. \tag{3.11}$$

In particular the kinetic-action is responsible for a diffusion of the random walk with a single particle variance equal to $\sigma^2_{ij}(\boldsymbol{r}) = 2\lambda\tau/g_{ij}(\boldsymbol{r})$. The inter-action is defined as $\mathscr{U} = \mathscr{S} - \mathscr{K}$ and for potential energies bounded from below one can resort to the Trotter formula [21] to reach the *primitive approximation* [5]

$$\mathscr{U}(R, R'; \tau) = \tau[V(R) + V(R')]/2. \tag{3.12}$$

Given then an observable $\mathscr{O}$ we can determine its thermal average at an absolute temperature T from

$$\langle\mathscr{O}\rangle = g_s{\rm tr}\{\rho(\beta)\mathscr{O}\}/Z_N, \tag{3.13}$$

$$Z_N = g_s{\rm tr}\{\rho(\beta)\}, \tag{3.14}$$

---

[2] The factor depending on the curvature of the manifold is due to Bryce DeWitt [18]. For a space of constant curvature there is clearly no effect, as the term due to the curvature just leads to a constant multiplicative factor that has no influence on the measure of the various observables.

Contracting Einstein field equations in vacuum implies a vanishing scalar curvature, the trace of Ricci tensor. Then Einstein field equations in vacuum reduce to the vanishing of the Ricci tensor. Therefore also the scalar curvature of a spatial foil, at constant time of Schwarzschild metric must vanish.

[3] Remember that the metric tensor is covariantly constant.

[4] The expression for $\mathscr{K}$ is the one of Eq. (24.16) of Ref. [20] to lowest order in $R - R'$.

[5] See Ref. [8] for a numerical analysis of the accuracy of this approximation and for its possible refinements.

where $\beta = 1/T$, $\mathrm{tr}\{\ldots\}$ is the trace over the spatial variables, Z_N the canonical partition function, $g_s = 2s+1$ is the spin degeneracy, and we assumed the Hamiltonian independent from spin. For *identical* bodies the spin-statistics theorem of quantum field theory, dictates that in spatial dimension bigger than two, particles with integer spin are bosons (obeying Bose-Einstein statistics, symmetric wavefunctions), while half-integer spin particles are fermions (obeying Fermi-Dirac statistics, antisymmetric wavefunctions). We will only consider polarized electrons that are fermions with $g_s = 1$.

The position representation of the density matrix at an imaginary time $t = \beta$ is obtained through a *path integral*

$$\rho(R, R'; \beta) = \langle R|\rho(\beta)|R'\rangle = \int \rho(R_0, R_1; \tau) \prod_{k=1}^{M-1} \left[\rho(R_k, R_{k+1}; \tau)\sqrt{\tilde{g}(R_k)}\, dR_k\right] \delta(R_0 - R)\delta(R_M - R')\, dR_0 dR_M, \tag{3.15}$$

where we have discretized the imaginary time β into M *timeslices* with a small *timestep* $\tau = \beta/M$. The volume element of integration, $\sqrt{\tilde{g}(R)}\, dR$, can be treated by introducing $W(R) = -[\ln\sqrt{\tilde{g}(R)}]/\tau$ as an effective *geometrical potential*. The many body path $R(t)$ is consequently discretized in M *beads* $R_k = (\{\boldsymbol{r}_{l,k}\}) = (\{r^j_{l,k}\})$ at each timeslice $k = 1, 2, \ldots, M$. We will also call *link* a pair of contiguous beads. Note that in order to measure an observable through Eq. (3.13) it is necessary to consider closed paths such that $R(t+\beta) = R(t)$, or rings on the foil.

For identical electrons, that satisfy to the Fermi-Dirac statistics, one needs to antisymmetrize the distinguishable density matrix (3.15) [22]. In these cases we can then write [6]

$$\rho_{\mathrm{F}}(R, R'; \beta) = \frac{1}{N!}\sum_{\mathscr{P}} \mathrm{sgn}(\mathscr{P})\rho(\mathscr{P}R, R'; \beta), \tag{3.16}$$

$$\mathrm{sgn}(\mathscr{P}) = (-1)^{\sum_{\nu=1}^{N}(\nu-1)C_\nu}, \tag{3.17}$$

where $\mathscr{P}$ is any permutation of the N particles such that $\mathscr{P}R = (\boldsymbol{r}_{\mathscr{P}1}, \boldsymbol{r}_{\mathscr{P}2}, \ldots, \boldsymbol{r}_{\mathscr{P}N})$, with sign $\mathrm{sgn}(\mathscr{P})$. Any permutations can be broken into cycles $\mathscr{P} = \{C_\nu\}$ where C_ν is the number of cycles of length ν in $\mathscr{P}$. An even (odd) permutation has $\mathrm{sgn}(\mathscr{P}) = +1(-1)$ and an even (odd) number of exchanges of a pair of particles.

We will model the Coulomb plasma in the white dwarf atmosphere as an electron gas of N electrons, i.e. a jellium where initially we neglect the uniform neutralizing background [7]. The Coulomb potential energy is then

$$V(R) = \sum_{m<n} \phi(\boldsymbol{r}_m, \boldsymbol{r}_n), \tag{3.19}$$

with ϕ the Coulomb pair potential between a charge q_m at $\boldsymbol{r}_m$ and a charge q_n at $\boldsymbol{r}_n$. The exact analytical expression for ϕ is given by the Copson-Linet potential [23–25] [8]

$$\phi(\boldsymbol{r}_1, \boldsymbol{r}_2) = \frac{q_1 q_2}{r_1 r_2}\left[\frac{(r_1 - \mathscr{M})(r_2 - \mathscr{M}) - \mathscr{M}^2\cos\gamma_{12}}{\sqrt{(r_1 - \mathscr{M})^2 + (r_2 - \mathscr{M})^2 - 2(r_1 - \mathscr{M})(r_2 - \mathscr{M})\cos\gamma_{12} - \mathscr{M}^2\sin^2\gamma_{12}}} + \mathscr{M}\right], \tag{3.20}$$

where

$$\cos\gamma_{12} = \sin\theta_1\sin\theta_2 + \cos\theta_1\cos\theta_2\cos(\varphi_1 - \varphi_2), \tag{3.21}$$

and the Linet topological term $q_1 q_2 \mathscr{M}/r_1 r_2$ is an isotropic, long-range, mutual energy correction ensuring that the presence of the Schwarzschild singularity doesn't introduce unphysical net charge accumulation [9]. In our white dwarf scenario, in Planck units, $\mathscr{M} \sim 10^{38} \ll \mathscr{R} \sim 10^{40}$ and this term will be small. In the flat spacetime $\mathscr{M} \to 0$

$$\phi(\boldsymbol{r}_1, \boldsymbol{r}_2) \to \frac{q_1 q_2}{\sqrt{r_1^2 + r_2^2 - 2r_1 r_2\cos\gamma_{12}}}. \tag{3.23}$$

---

[6] One can antisymmetrize respect to the first, the second, or both the arguments of the distinguishable density matrix. We here choose the first case.

[7] In a jellium Eq. (3.19) should be substituted by

$$V(R) = \sum_m \phi_b(r_m) + \sum_{m<n} \phi(\boldsymbol{r}_m, \boldsymbol{r}_n), \tag{3.18}$$

with ϕ_b the potential energy due to the uniform proper charge density $\rho_b = -ne$ of the neutralizing background as described in Section IV A. Since ϕ_b is just a shallow harmonic pull at the center of the patch we will initially neglect it.

[8] Compare with the one on a Flamm paraboloid [26].

[9] Note that since the angular distances are extremely small, for example of the order of 10^{-17} in case A of Table I, we can use the following approximation

$$\phi(\boldsymbol{r}_1, \boldsymbol{r}_2) = \frac{q_1 q_2}{r_1 r_2}\left[\frac{(r_1 - \mathscr{M})(r_2 - \mathscr{M}) - \mathscr{M}^2}{\sqrt{(r_1 - r_2)^2 + 2(r_1 - \mathscr{M})(r_2 - \mathscr{M})(1 - \cos\gamma_{12})}} + \mathscr{M}\right], \tag{3.22}$$

where we may expand $\cos\gamma - 1$ to first order in θ_i, φ_i. We are allowed to approximate the $cos\gamma_{12} \approx 1$ in the numerator since $\mathscr{M}\theta_0^2/\mathscr{R} \sim 10^{-36}$. We are also allowed to neglect the term $\mathscr{M}^2\sin^2\gamma_{12}/\mathscr{R}^2 \approx (\mathscr{M}\theta_0/\mathscr{R})^2 \sim 10^{-39}$. Note that on a computer in order to be able to calculate the difference $r_1 - r_2$ between two electrons of the patch we need quadruple precision since $\mathscr{R} \sim 10^{40}$ and $\delta \sim 10^{23}$ so we need at least 17 significant digits. Since we have wall boundary conditions on r and periodic boundary conditions on θ, φ, in order to fulfill the minimum image convention, given θ_1, φ_1 we will choose the image of θ_2, φ_2 which gives the minimum $1 - \cos\gamma_{12}$.

IV. PIMC CONSTRAINED IN A PATCH OF A RADIAL THIN SURFACE LAYER

From exercise 4.1 of the book [1] follows that the depth of the thin radiating surface layer of a white dwarf is

$$\mathscr{D} \lesssim 10^{-2}\mathscr{R}, \tag{4.1}$$

where the typical radius of a white dwarf is $\mathscr{R} \approx 10^{-3}R_\odot - 10^{-2}R_\odot$.

In order to treat the problem of electrons constrained in a subatomic patch of a thin spherical shell of width $\delta \ll \mathscr{D}$ we imagine an infinite repulsive external potential at $r > \mathscr{R}$ and at $r < \mathscr{R} - \delta$ In the Monte Carlo we reject any move that brings an electron in these regions in oredr to simulate wall boundary conditions on r. On the other hand we will adopt periodic boundary conditions on θ and φ with periodicities θ_0 and φ_0 respectively. We will choose $\theta_0 = \varphi_0$. We want the radial extent of the patch comparable to the angular extent so we will choose $\delta \approx \mathscr{R}\theta_0$.

Of course this is a first brute approximation to a more realistic model including an 'osmosis' of electrons between the patch of the white dwarf atmosphere and the star interior. Using periodic boundary conditions on the spherical angles we model a thin spherical shell of radial width δ. Even if we will not worry about finite size errors which occur inevitably due to the choice of $\theta_0 \ll \pi/2$.

The Cartesian coordinates of a particle on the Schwarzschild spatial foil is

$$\begin{cases} x = r\cos\theta\cos\varphi \\ y = r\cos\theta\sin\varphi \\ z = r\sin\theta \end{cases} \tag{4.2}$$

where $r^1 = r \in [\mathscr{R} - \delta, \mathscr{R}]$, $r^2 = \theta \in [-\theta_0/2, \theta_0/2]$ with $\theta = 0$ a Flamm paraboloid equatorial section of the spatial foil, $r^3 = \varphi \in [-\varphi_0/2, \varphi_0/2]$, and the particle path on it is $\boldsymbol{q}(t) = (x(t), y(t), z(t))$. The angular extent of the patch θ_0 is such that

$$\Omega = \Omega_r 2\sin\left(\frac{\theta_0}{2}\right)\varphi_0 \approx \Omega_r\theta_0^2 = N/n, \tag{4.3}$$

where Ω is the volume of the patch and $\Omega_r = \frac{4\pi}{3}\left[\mathscr{R}^3 - (\mathscr{R} - \delta)^3\right]$.

In natural Planck units $e^2 = 0.00729735$. Under the experimental conditions of case A of Table I we estimate that the magnitude of the geometrical potential $\sim (1/\beta)\ln(\mathscr{R}^2) \sim 10^{-24}$ is just one order of magnitude larger than the gravitational potential $Gm\mathscr{M}/\mathscr{R} \sim 10^{-25}$ that we will neglect. On the other hand, introducing the Wigner-Seitz radius $r_s = (4\pi n/3)^{-1/3}/a_0$ with $a_0 = \hbar^2/me^2$ the Bohr radius, the Copson-Linet pair potential $\sim e^2/a_0 r_s \sim 10^{-26}$ is just one order of magnitude smaller than the gravitational potential. The kinetic energy is one order of magnitude less, $\sim m(r_s/\beta)^2 \sim 10^{-27}$.

A. Effect of the neutralizing background

The charge neutrality of the jellium in the patch requires

$$\rho_b = -\frac{Ne}{\Omega} = -ne, \tag{4.4}$$

Neglecting the angular dependence of the electric field in the patch, the Poisson equation for the background potential energy ϕ_b is

$$\frac{1}{r^2}\frac{d}{dr}\left[r^2\sqrt{1 - R_{\rm Sc}/r}\,E\right] = -4\pi\rho_b, \tag{4.5}$$

where $E(r) = -d\phi_b(r)/dr$ is the radial electric field. Integrating the Poisson equation from $r = R_{\rm in} = \mathscr{R} - \delta/2$ to r yields the internal electric field

$$E(r) = -\frac{4\pi\rho_b}{3}\frac{r^3 - R_{\rm in}^3}{r^2\sqrt{1 - R_{\rm Sc}/r}}, \tag{4.6}$$

where we chose $E(R_{\rm in})=0$. Integrating $E(r)$ from $r=R_{\rm in}$ to r yields the background potential profile

$$\begin{aligned}\phi_b(r)=-\frac{8\pi e\rho_b}{3}\Bigg\{&\frac{1}{2}\left[\sqrt{r^3(r-R_{\rm Sc})}-\sqrt{R_{\rm in}^3(R_{\rm in}-R_{\rm Sc})}\right]+\\&\frac{2R_{\rm in}^3}{R_{\rm Sc}}\left[\sqrt{1-R_{\rm Sc}/R_{\rm in}}-\sqrt{1-R_{\rm Sc}/r}\right]+\\&\frac{3R_{\rm Sc}}{4}\left[\sqrt{r(r-R_{\rm Sc})}-\sqrt{R_{\rm in}(R_{\rm in}-R_{\rm Sc})}\right]+\\&\frac{3R_{\rm Sc}^2}{4}\left[\operatorname{atanh}\sqrt{1-R_{\rm Sc}/r}-\operatorname{atanh}\sqrt{1-R_{\rm Sc}/R_{\rm in}}\right]\Bigg\},\end{aligned}\tag{4.7}$$

Which reduces to the usual quadratic potential $\phi_b(r)\to-8\pi e\rho_b(r-R_{\rm in})^2(r+2R_{\rm in})/3r$ in the flat $R_{\rm Sc}\to 0$ limit, where we grounded the surface $r=R_{\rm in}$. The order of magnitude of the background potential for each charge is $\sim e^2n\delta^2\sim 10^{-26}$. For simplicity we will neglect the periodic angular images of the electrons [27]. For case A of Table I we measured $Ne_K=1.578(7)\times 10^{-24}$ and $Ne_V=4.9458(7)\times 10^{-23}$. So the effect of the background is to increase both the kinetic and potential energy of the plasma.

B. The black hole limit

It is interesting to study the limit of the black hole $R_{\rm Sc}\to\mathscr{R}$ or $\mathscr{M}\to\mathscr{R}/2$, keeping all other parameters fixed. By doing so we imagine a star with a mass increasing up to the point in which its Schwarzschild radius coincides with its radius. So that the star becomes a black hole. In this mathematical limit the geometrical potential diverges to $-\infty$ and, assuming that all the particles are sitting on the horizon at $r=\mathscr{R}$, the Copson pair potential (3.20) reduces to $\phi\to q_1q_2/\mathscr{R}$, independently of their distance.

In order to get a feeling of the plasma behavior approaching the mathematical black hole limit, in our simulations we will increase the mass of the star so that, respect to the realistic white dwarf scenario, the geometrical potential will become more negative and the Copson potential will be diminished.

V. NUMERICAL RESULTS

We will choose as reference system (case A of Table I) a white dwarf with $\mathscr{R}=R_\odot 10^{-3}$, $\mathscr{M}=M_\odot$, with an atmosphere with $n=3\times 10^{-72}$, $T=10^6$K. We will zoom on the patch described in the previous section with $r\in[\mathscr{R}-\delta,\mathscr{R}]$, $\theta\in[-\theta_0/2,\theta_0/2]$, and $\varphi\in[-\theta_0/2,\theta_0/2]$ with the radial width $\delta\approx\mathscr{R}\theta_0$. We will use just $N=30$ electrons of the atmosphere and we will choose $\delta=R_\odot 10^{-20}$ and $\theta_0=10^{-17}$ according to (4.3).

We use the Metropolis algorithm [28, 29] to evaluate the average of Eq. (3.13).

In order to explore ergodically the positions space $\boldsymbol{r}=(r,\theta,\varphi)$ to sample the distinguishable density matrix we use the transition *displacement* move described in Appendix A of Ref. [15].

In order to sample the permutation sum of Eq. (3.16) needed for fermions we use a transition move combination of 2 Brownian *bridges* between unlike electrons as described in Appendix B of Ref. [15]. To construct a single Brownian bridge it is essential to map, project, the Schwarzschild spatial foil on a flat coordinate system. Our choice is presented in Appendix B of Ref. [15]. Perform the Gaussian bridge move in the projection flat space and then map it back to the Schwarzschild spatial foil. The Metropolis algorithm will then allow to sample the high temperature density matrix whose kinetic action is not purely Gaussian on the Schwarzschild spatial foil, due to the metric tensor appearing in $d\tilde{s}^2$.

We will work in the canonical ensemble with fixed number of particles N, electron number density $n=-\rho_b/e$, and absolute temperature $T=1/k_B\beta$. The jellium *degeneracy parameter* is $\Theta=T/T_D$ where the degeneracy temperature $T_D=n^{2/3}\hbar^2/mk_B$ [10]. For temperatures higher than T_D, $\Theta\gg 1$, quantum effects are not very important. The *Coulomb coupling constant* is $\Gamma=\beta e^2/a_0r_s$. At weak coupling, $\Gamma\ll 1$. The plasma becomes weakly correlated at high r_s in the classical regime, $\Theta\gg 1$, and at low r_s in the quantum regime, $\Theta\ll 1$, since the kinetic energy scales as $1/r_s^2$ and the potential energy as $1/r_s$.

---

[10] This is the temperature at which the size of a single electron path, in absence of interaction, i.e. the thermal wavelength $(2\lambda\beta)^{1/2}$, equals the separation between single particle paths, i.e. roughly $n^{-1/3}$. Below this temperature it is possible for single particle paths to link up exchanging their end points.

In Table I we report the cases studied. We keep the electrons number density $n = 3 \times 10^{26}\text{cm}^{-3}$, the number of electrons $N = 30$, and the patch geometry fixed and we vary the temperature. As we can see from the values of r_s, Γ, and Θ for cases A, B, C the atmosphere is expected to be in the quantum regime and weakly correlated. Case M is like case A but with $\mathscr{M} = 0$ so that the geometrical effect of gravity is canceled. Case BH is like case A but with $\mathscr{M} = 10^{40}$ so that the Schwarzschild radius comes closer to the plasma by ≈ 110 solar masses.

TABLE I. Cases treated in our simulations: $\mathscr{R}$ the white dwarf radius, δ the patch radial width, $\mathscr{M}$ the white dwarf mass, N the number of particles, r_s the Wigner-Seitz radius, β the inverse temperature. The adimensional quantities Γ and Θ were introduced in the main text. The results for the thermodynamic quantities, $e_K = \langle K\rangle/N$ from the thermodynamic estimator $K(R,R';\tau) = \tilde{g}_{\mu\nu}(R)(R-R')^\mu(R-R')^\nu/4\lambda\tau^2$ as explained in Ref. [8], $e_V = \langle V\rangle/N$ the Coulomb potential energy per particle, and $e_W = \langle W\rangle/N$ the geometrical potential energy per particle, are given for the simulation without the sum over the permutations in Eq. (3.16) and with the permutations sum in the bottom table. In the RPIMC case we also report the average number of two particles exchanges $< N$. We neglected the presence of the neutralizing background of Section IV A. We chose natural Planck units with $c = G = \hbar = k_B = 1$. The simulation lasted not less than 10^5 Monte Carlo steps where one step is made of a displace move of all the beads of a single particle path as described in Appendix A of Ref. [15] and a bridge move as described in Appendix B of Ref. [15].

case	M	N	$\mathscr{R}$	δ	$\theta_0 = \varphi_0$	$\mathscr{M}$	β	$a_0 r_s$	r_s	Γ	Θ
A	30	30	$R_\odot 10^{-3}$	$R_\odot 10^{-20}$	10^{-17}	$M_\odot$	1.4×10^{26}	2×10^{23}	0.061	5.17	0.03
B	300	30	$R_\odot 10^{-3}$	$R_\odot 10^{-20}$	10^{-17}	$M_\odot$	1.4×10^{27}	2×10^{23}	0.061	51.7	0.003
C	3	30	$R_\odot 10^{-3}$	$R_\odot 10^{-20}$	10^{-17}	$M_\odot$	1.4×10^{25}	2×10^{23}	0.061	0.517	0.3
M	30	30	$R_\odot 10^{-3}$	$R_\odot 10^{-20}$	10^{-17}	0	1.4×10^{26}	2×10^{23}	0.061	5.17	0.03
BH	30	30	$R_\odot 10^{-3}$	$R_\odot 10^{-20}$	10^{-17}	$109.4 M_\odot$	1.4×10^{26}	2×10^{23}	0.061	5.17	0.03

	PIMC no permutations			RPIMC with permutations			
case	$Ne_K(\times 10^{-24})$	$Ne_V(\times 10^{-23})$	$-Ne_W(\times 10^{-21})$	# swaps	$Ne_K(\times 10^{-24})$	$Ne_V(\times 10^{-23})$	$-Ne_W(\times 10^{-21})$
A	1.627(2)	4.6549(1)	1.178895	25.6(2)	1.637(3)	4.6550(2)	1.178895
B	1.635(3)	4.6546(2)	1.178895	20.3(6)	1.644(4)	4.6548(3)	1.178895
C	1.605(2)	4.6548(1)	1.178895	26.01(3)	1.643(3)	4.6549(2)	1.178895
M	–	–	–	26.0(1)	1.627(2)	4.6548(2)	1.178881
BH	–	–	–	26.1(1)	2.104(4)	4.2502(2)	1.180852

Apart from thermodynamic properties like the *kinetic energy* per particle, const $- e_K > 0$, the *Coulomb potential energy* per particle, e_V, [11] and the *geometrical potential energy* per particle, e_W, we will also measure structural properties like the *radial distribution function* (RDF), $g(r) = \langle \mathscr{O}\rangle$. For it we used the following histogram estimator,

$$O(R;r,a) = \sum_{m\neq n} \frac{1_{]r-\Delta/2,r+\Delta/2]}(d_{mn})}{N n_{id}(r)}, \tag{5.1}$$

where Δ is the histogram bin, $1_{]u,v]}(x) = 1$ if $x \in]u,v]$ and 0 otherwise, d_{mn} is the Euclidean distance between 2 electrons m, n [12]

$$d_{mn} = d(\boldsymbol{r}_m, \boldsymbol{r}_n) = \sqrt{(\boldsymbol{q}_n - \boldsymbol{q}_m)\cdot(\boldsymbol{q}_n - \boldsymbol{q}_m)}, \tag{5.2}$$

and

$$n_{id}(r) = 4\pi n\left[(r+\Delta/2)^3 - (r-\Delta/2)^3\right]/3\ , \tag{5.3}$$

is the average number of particles on the spherical shell $]r-\Delta/2, r+\Delta/2]$ for the ideal gas of density n. We have that $n^2 g(r)$ gives the probability, that sitting on a particle at $\boldsymbol{r}$, one finds another particle at $\boldsymbol{r}'$ with $r = d(\boldsymbol{r}, \boldsymbol{r}')$.

[11] The estimators for these observables are carefully described in Ref. [8].
[12] Here it is important to expand $\cos\gamma_{mn} - 1$ of Eq. (3.21) at least to second order in θ_i, φ_i for $i = n, m$ in order to have the correct behavior of the RDF at small distances.

Fermions properties cannot be calculated exactly with path integral Monte Carlo because of the *fermions sign problem* [22, 30]. We then have to resort to an approximate calculation. The one we chose was the Restricted Path Integral (RPIMC) approximation [13, 22, 30, 31] with a "free fermions restriction". The trial density matrix used in the *restriction* is chosen as the one reducing to the ideal density matrix in the limit of $t \ll 1$ and is given by the following explicit analytic expression,

$$\rho_0(R', R; t) \propto \det \left\| e^{-\frac{d^2(\mathbf{r}'_{i,k}, \mathbf{r}_{j,l})}{4\lambda t}} \right\|. \tag{5.4}$$

Note that here we purposely chose the Euclidean distance (5.2). We did this just for the sake of simplicity. In any case both the Euclidean and the geodesic distance reduce to $ds^2(\mathbf{r}_{i,k}, \mathbf{r}_{j,l}) = g_{\alpha\beta}(\mathbf{r}_i)(\mathbf{r}_{i,k} - \mathbf{r}_{j,l})^\alpha(\mathbf{r}_{i,k} - \mathbf{r}_{j,l})^\beta$ in the $t = \tau|k-l| \ll 1$ limit. The implementation of the RPIMC on a curved space has already been described in section IV B of Ref. [15]. The permutation sampling necessary to compute the sum in Eq. (3.16) is carried out through the composition of two Brownian bridges and a swap of two identical particles (we explicitly neglected 3 particles permutation cycles). The realization of a Brownian bridge on the curved Schwarzschild space used a mapping onto a flat space as explained in appendix B of Ref. [15] with the only care of distinguishing between a radial standard deviation $\sigma_r = \sqrt{2\lambda\tau}$ and an angular one $\sigma_a = \sigma_r/\mathscr{R}$ for the Gaussian in the flat projected space (r, θ, φ).

We start the simulation with random beads of each electron at each timeslice within the subatomic patch. In case A of Table I we simulate the white dwarf at different temperatures: $T = 10^6$K, in case B $T = 10^5$K, and in case C $T = 10^7$K. Case M is like case A but in absence of with $\mathscr{M} \to 0$. And case BH is like case A but with a larger mass of the star approaching the black hole limit described in Section IV B. In all cases we keep a fixed timestep $\tau = \beta/M = 4.7 \times 10^{24}$ in Planck units. For each case we use either the PIMC treating the electrons as Boltzmannons, neglecting the permutations sum in Eq. (3.16) and the RPIMC which correctly but approximately treats the electrons as Fermions.

From the table we see how the potential, Coulomb or geometrical, does not change appreciably between cases A,B,C. On the other hand, the kinetic energy increases with temperature in the simulations without the permutations and has less variations in the RPIMC simulations. Quantum statistics affects Ne_K by $\sim 1\%$. And Ne_K diminishes when RPIMC is used. The relative difference of the geometrical potential of case A and M is $\sim 10^{-5}$ while the kinetic energy relative difference is already $\sim 10^{-2}$. Approaching the black hole limit the geometrical potential becomes more negative, the Copson potential is lowered, and the kinetic energy diminishes. This is shown by comparing cases A and BH of the Table.

In Fig. 1 we show the RDF for the three cases A,B,C of Table I without the electrons permutations. The peak of the RDF is at a distance $\Delta r \approx a_o r_s/4 \sim 10^{23} \times 10^{-33}$cm $\sim 10^{-2}$Å. This means that two electrons are likely to be found closer than the Wigner-Seitz radius. From the figure we see how $g(r \to 0) \to 0$ in agreement with the divergence of the Coulomb potential when the two electrons coincide. The patch geometry accommodates just the first oscillation of the RDF which otherwise would tend to $g(r \to \infty) \to 1$. The extremely high peak can be explained as due to the geometry of the patch. Compare with the RDF of Euclidean jellium in a periodic cubic box [16]. We see how the change in temperature does not produce an appreciable change in the RDF. The same can be said for the effect of the Fermi statistics or the geometrical effect of gravity.

In Fig. 2 we show a snapshot of the electrons paths in the coordinates (r, θ, φ) in the plasma for the patch of case A with RPIMC of Table I at thermal equilibrium.

VI. CONCLUSIONS

Still largely unknown is the process of cooling of a white dwarf. We think that the dead star still possesses some activity in its thin radiating atmospheric layer. Which is the source of the luminosity that we are able to measure. It is therefore important to be able to understand the properties, thermodynamic and structural, of the plasma that forms the atmosphere.

In this brief work we simulated a subatomic patch of this layer. We modeled the plasma as a jellium where we initially neglect the effect of the uniform neutralizing background. For the Coulomb pair potential between the electrons we adopted the Copson solution for particles living in a spatial section of the Schwarzschild metric. We modeled the patch of the dimensions of Å/20 using periodic boundary conditions on the spherical angles and wall boundary conditions on the redial coordinate. The expected experimental conditions of the plasma suggest that it will be weakly interacting and the quantum statistics will play a non negligible role. Therefore we used the path integral method to estimate the quantum effects. We found that quantum statistics affects the third significant figure of the kinetic energy. We then used the Schwarzschild solution of Einstein field equations to estimate the geometrical effect of gravity. These also affect the third significant figure of the kinetic energy. Our measure of the radial distribution function does not feel appreciably none of these effects, temperature, quantum statistics, or gravity.

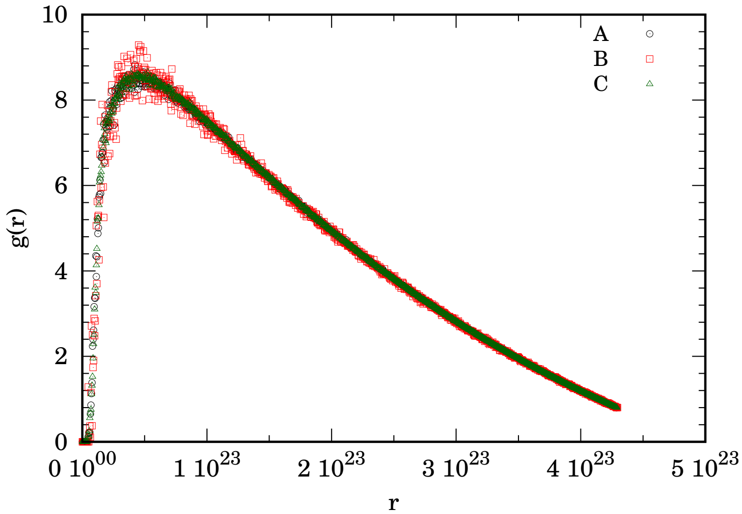

FIG. 1. The RDF for cases A,B,C of Table I without permutations. We explicitly verified that taking into account the permutations among the electrons does not change appreciably the RDF. The RDFs of cases M and BH are also not appreciably different from the one of case A shown here. The radial distance r is in Planck units 1.61623×10^{-33}cm. The radial length of the patch is $\delta = 4.3 \times 10^{23}$.

We then imagined a situation where we increase the mass of the star keeping all other parameters constant so to let the event horizon come closer to the patch and we noticed a diminution of both the kinetic and the potential energy of the plasma. Both the geometrical and the Coulomb potential energies diminish.

Comparing with the phase diagram of jellium in Euclidean space we see how in our case A we are on the lower left corner of figure 1 of Ref. [16] so that in order to see a crystallization we should at the same time wait for the star to cool down and observe the outer more rarefied part of the atmosphere.

AUTHOR DECLARATIONS

Conflicts of interest

None declared.

Data availability

The data that support the findings of this study are available from the corresponding author upon reasonable request.

Funding

None declared.

---

[1] S. L. Shapiro and S. A. Teukolsky, *Black Holes, White Dwarfs, and Neutron Stars. The Physics of Compact Objects* (John Wiley & Sons Inc, New York, 1983).
[2] S. Chandrasekhar and E. A. Milne, The Highly Collapsed Configurations of a Stellar Mass, Monthly Notices of the Royal Astronomical Society **91**, 456 (1931).
[3] S. Chandrasekhar, The Density of White Dwarf Stars, Phil. Mag. **11**, 592 (1931).

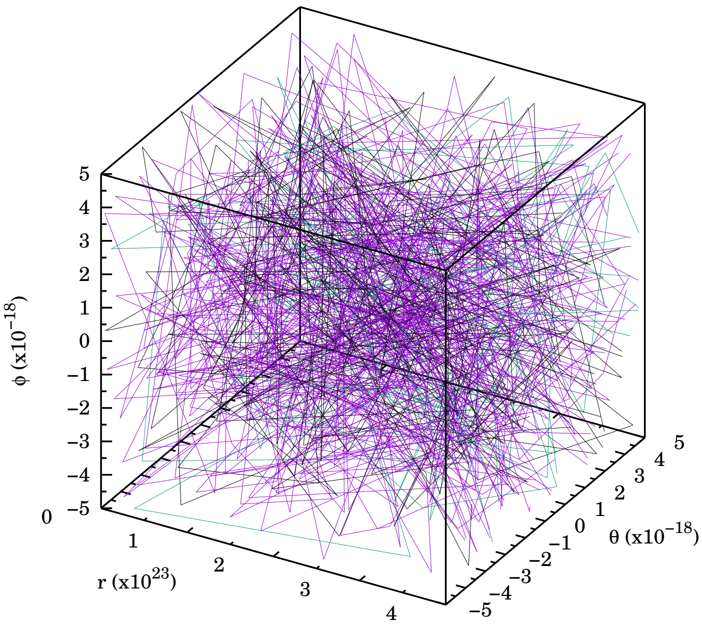

FIG. 2. Snapshot of the Coulomb plasma of case A of Table I with permutations. The radial distance r is in Planck units 1.61623×10^{-33}cm. The paths of the 30 electrons are painted with different colors for different permutations cycles.

[4] S. Chandrasekhar, The Maximum Mass of Ideal White Dwarfs, Astrophys. J. **74**, 81 (1931).

[5] R. Fantoni, White-dwarf equation of state and structure: the effect of temperature, J. Stat. Mech. , 113101 (2017).

[6] R. C. Tolman, Static Solutions of Einstein's Field Equations for Spheres of Fluid, Phys. Rev. **55**, 364 (1939).

[7] J. R. Oppenheimer and G. M. Volkoff, On Massive Neutron Cores, Phys. Rev. **55**, 374 (1939).

[8] D. M. Ceperley, Path integrals in the theory of condensed Helium, Rev. Mod. Phys. **67**, 279 (1995).

[9] R. Arnowitt, S. Deser, and C. Misner, The Dynamics of General Relativity, In: Witten, L., Ed., Gravitation: An Introduction to Current Research, Wiley & Sons, New York, 227 (1962), arXiv: gr-qc/0405109.

[10] R. Fantoni, Formalism for the Matter Density Matrix in an ADM $3+1$ foliation of spacetime, Phys. Rev. Lett. (in preparation) (2026), `https://rfantoni.github.io/personal-page/publications/pcdms.pdf`.

[11] R. C. Tolman, On the Weight of Heat and Thermal Equilibrium in General Relativity, Phys. Rev. **35**, 904 (1930).

[12] R. C. Tolman and P. Ehrenfest, Temperature Equilibrium in a Static Gravitational Field, Phys. Rev. **36**, 1791 (1930).

[13] R. Fantoni, One-component fermion plasma on a sphere at finite temperature, Int. J. Mod. Phys. C **29**, 1850064 (2018).

[14] R. Fantoni, One-component fermion plasma on a sphere at finite temperature. The anisotropy in the paths conformations, J. Stat. Mech. , 083103 (2023).

[15] R. Fantoni, Path Integral Monte Carlo on a Sphere, Phys. Rev. B **114**, 185409 (2026).

[16] E. W. Brown, B. K. Clark, J. L. DuBois, and D. M. Ceperley, Path-Integral Monte Carlo Simulation of the Warm Dense Homogeneous Electron Gas, Phys. Rev. Lett. **110**, 146405 (2013).

[17] R. Fantoni, Statistical Gravity, ADM splitting, and Affine Quantization, Gravitation and Cosmology **31**, 568 (2025).

[18] B. S. DeWitt, Dynamical Theory in Curved Spaces. I. A Review of the Classical and Quantum Action Principles, Rev. Mod. Phys. **29**, 377 (1957).

[19] J. H. V. Vleck, The Correspondence Principle in the Statistical Interpretation of Quantum Mechanics, Proc Natl Acad Sci U S A **14**, 178 (1928).

[20] L. S. Schulman, *Techniques and Applications of Path Integration* (John Wiley & Sons, Technion, Haifa, Israel, 1981) chapter 24.

[21] H. F. Trotter, On the Product of Semi-Groups of Operators, Proc. Am. Math. Soc. **10**, 545 (1959).

[22] D. M. Ceperley, Path integral Monte Carlo methods for fermions, in *Monte Carlo and Molecular Dynamics of Condensed Matter Systems*, edited by K. Binder and G. Ciccotti (Editrice Compositori, Bologna, Italy, 1996).

[23] E. T. Copson, On electrostatics in a gravitational field, Proceedings of the Royal Society of London **118**, 184 (1928).

[24] B. Linet, Electrostatics and magnetostatics in the Schwarzschild metric, Journal of Physics A: Mathematical and General **9**, 1081 (1976).

[25] B. Linet, Electrostatic self-force and material sources of the gravitational field, General Relativity and Gravitation **18**, 731 (1986).
[26] R. Fantoni and G. Téllez, Two dimensional one-component plasma on a Flamm's paraboloid, J. Stat. Phys. **133**, 449 (2008).
[27] V. Natoli and D. M. Ceperley, An Optimized Method for Treating Long-Range Potentials, Comput. Phys. **117**, 171 (1995).
[28] N. Metropolis, A. W. Rosenbluth, M. N. Rosenbluth, A. M. Teller, and E. Teller, Equation of state calculations by fast computing machines, J. Chem. Phys. **1087**, 21 (1953).
[29] M. H. Kalos and P. A. Whitlock, *Monte Carlo Methods* (John Wiley & Sons Inc., New York, 1986).
[30] D. M. Ceperley, Fermion Nodes, J. Stat. Phys. **63**, 1237 (1991).
[31] R. Fantoni, Jellium at finite temperature, Mol. Phys. **120**, 4 (2021).